Journal of Drug Delivery Science and Technology 89 (2023) 105057

Contents lists available at ScienceDirect

Journal of Drug Delivery Science and Technology

journal homepage: www.elsevier.com/locate/jddst

Evaluation of the potential of chitosan-based films with α,β-amyrenone triterpene for wound healing

Ulana Cristina de Araújo Tavares [a], Juliana Maria Nascimento dos Santos [a], Sávio Gorgônio Paes de Bulhões [a], Lucas Gabriel de Medeiros da Silva [a], Verônica da Silva Oliveira [a], Emanuella de Aragão Tavares [a], Raimundo Fernandes de Araújo Júnior [b], Valéria Costa da Silva [c], Gerlane Coelho Bernardo Guerra [c], Emerson Silva Lima [d], Valdir Florêncio da Veiga Júnior [e], Attilio Converti [f], Ádley Antonini Neves de Lima [a,*]

[a] Department of Pharmacy, Health Center, Federal University of Rio Grande do Norte, 59012-570, Natal, RN, Brazil
[b] Department of Morphology, Federal University of Rio Grande do Norte, 59072-970, Natal, RN, Brazil
[c] Department of Biophysics and Pharmacology, Biosciences Center, Federal University of Rio Grande do Norte, 59072-970, Natal, RN, Brazil
[d] Department of Pharmacy, Biological Activity Laboratory, Federal University of Amazonas, 69077-000, Manaus, Am, Brazil
[e] Department of Chemistry, Institute of Exact Sciences, Federal University of Amazonas, 69077-000, Manaus, Am, Brazil
[f] Department of Civil, Chemical and Environmental Engineering, University of Genoa, I-16145, Genoa, Italy

ARTICLE INFO

Keywords:
Chitosan films
Triterpenes
α,β-amyrenone
Anti-inflammatory
Wound healing

ABSTRACT

α,β-Amyrenone (ABAME) is a mixture of natural isomers belonging to the class of triterpenes, which have great potential because of their biological activities, mainly the anti-inflammatory one. Chitosan films are increasingly used for topical use because they enable a gradual release of the drug, in addition to many other advantages. Therefore, the goal of this study was to develop ABAME-containing chitosan films, aiming at the topical application in the treatment of skin lesions. ABAME films were submitted to physicochemical characterization and assessed for *in vivo* wound healing. Thermal analysis and FTIR suggested ABAME incorporation into the chitosan matrix, while XRD showed characteristic halos of amorphous compounds, indicating ABAME amorphization by chitosan. SEM images confirmed its homogeneous inclusion in chitosan matrix, with partial loss of pure ABAME crystallinity. In the *in vivo* tests, the groups CF1, CF2 and CF5, treated with chitosan films with different ABAME concentrations, exhibited a more efficient and faster regeneration process than the other groups, mainly after 7 and 10 days of treatment. In the histopathological tests, chitosan-ABAME films showed a reduction in inflammatory infiltrates, greater neovascularization, re-epithelialization, and absence of necrosis and costal points when compared to the untreated group and blank chitosan film. Additionally, the CF1, CF2 and CF5 groups showed a reduction in the NTF-α and IL-1β cytokines levels, as well as an increase in that of IL-10 compared to the untreated group after 7 and 14 days. ABAME-containing chitosan films were very efficient in the wound healing process, due to the anti-inflammatory properties of the active component; therefore, they may be used as a promising delivery system to treat skin lesions.

1. Introduction

Triterpenes are a class of natural compounds belonging to the group of terpenes, whose considerable pharmacological relevance is due to their great distribution in nature and the large number of their biological activities, including the anti-inflammatory [1,2], antimicrobial [3,4], antineoplastic [5–7], antiviral [8,9], antiparasitic [4,10], cardioprotective [11,12], hepatoprotective [8,13], nephroprotective [14],

* Corresponding author.
E-mail addresses: ulanatavares@gmail.com (U.C. de Araújo Tavares), juem.sm@gmail.com (J.M.N. dos Santos), saviopaes96@gmail.com (S.G.P. de Bulhões), lucasgmedeiros97@gmail.com (L.G. de Medeiros da Silva), veronicasoliver47@gmail.com (V. da Silva Oliveira), emanuella_ta@hotmail.com (E. de Aragão Tavares), fernandes.araujo@ufrn.br (R.F. de Araújo Júnior), vcs.biomed@gmail.com (V. Costa da Silva), gerlaneguerra@hotmail.com (G.C.B. Guerra), eslima@ufam.edu.br (E.S. Lima), valdir.veiga@gmail.com (V.F. da Veiga Júnior), converti@unige.it (A. Converti), adleyantonini@yahoo.com.br (Á.A. Neves de Lima).

https://doi.org/10.1016/j.jddst.2023.105057
Received 15 May 2023; Received in revised form 6 October 2023; Accepted 8 October 2023
Available online 14 October 2023

neuroprotective [15], hypoglycemic [16,17] and lipid-lowering ones, in addition to helping in the management of the metabolic syndrome [18]. In this context, these compounds are increasingly investigated in the health and pharmaceutical fields, seeking for new drug candidates [19].

α,β-Amyrenone (ABAME) (Fig. 1A) are triterpenoid isomers found in several oleoresins of Brazilian Amazonian species belonging to the genus *Protium* (Burseraceae). Particularly, the species *Protium heptaphyllum*, popularly known as "almecegueira", contains several triterpenes in the oily resin of its trunk, the most abundant of which are α,β-amyrin isomers [20,21]. ABAME can be obtained by oxidation of these compounds with a yield of approximately 65–85% [22].

Even though some *in vivo* studies have already demonstrated a significant anti-inflammatory activity of ABAME, they are a few and do not show the prototype in a pharmaceutical form [20].

Early studies reported the ability of ABAME to interfere in inflammatory processes and to inhibit neutrophil migration [23]. De Almeida et al. [24] reported that ABAME inhibited the productions of nitric oxide and interleukin 6 (IL-6), induced the production of interleukin 10 (IL-10) in murine macrophages stimulated by lipopolysaccharide, and reduced the cyclo-oxygenase-2 (COX-2) expression. Additionally, other studies carried out to understand the mechanism of action in metabolic diseases have proven inhibitory effects on lipase, α-glucosidase and α-amylase [20] as well as reduction of postprandial glycemia and obesity in mice [18].

The growing demand for new drugs able to ensure higher income, therapeutic activity and pharmacological efficacy has stimulated the search for plant-derived products [25–28].

Chitosan is a biopolymer obtained by the deacetylation of chitin, a natural biopolymer present in the exoskeleton of insects which is composed of β-(1 → 4)-2-amino-2-deoxy-D-glucose and β-(1 → 4)-2-acetamide-2-deoxy-D-glucose units (Fig. 1B). The degrees of deacetylation and impurities as well as molar mass distribution of chitosan depend on the natural source and the method of separation [29].

Chitosan films are very promising for the development of new drugs because they have low toxicity, are permeable to water and oxygen, are flexible, and do not break or tear easily. In addition, they allow a prolonged drug release and are biodegradable, thus managing to reduce the problems associated with drug disposal in the environment [30–34].

The importance of this study is the development of a new pharmaceutical form for the inclusion and skin administration of ABAME. For this purpose, ABAME-containing chitosan-based polymeric films were prepared, whose anti-inflammatory and wound healing potential were *in vivo* investigated. In other words, a directed application of this active compound has been sought in skin lesions, given that the preparation, investigation and application of an ABAME pharmaceutical form has not been mentioned in the literature so far.

2. Materials and methods

2.1. Materials

α,β-Amyrenone (ABAME) was obtained in partnership with the Federal University of Amazonas, while chitosan, with low molecular weight (50–190 kDa) and deacetylation degree of 75–85%, was acquired from Sigma Aldrich (São Paulo, SP, Brazil). All other reagents used were of analytical grade.

2.2. Films preparation

Films were prepared according to the sol-gel solvent evaporation method with some adaptations [35]. Briefly, a chitosan solution (1%, w/v) prepared in acetic acid (1% v/v) was subjected to magnetic stirring for 24 h and filtered under vacuum. Then, 7 ml of this solution were transferred to Petri dishes (diameter of 47 mm) and dried in an oven at 40 ± 2 °C overnight to obtain the blank chitosan film (BCF).

To develop chitosan-ABAME films, three ABAME solutions were prepared in ethanol at concentrations of 1, 2 and 5 mg/ml. Subsequently, 2 ml of each solution were added to 7 ml of the chitosan solution (1%, w/v), homogenized under stirring, transferred to Petri dishes (diameter of 47 mm), and then dried in an oven at 40 ± 2 °C for 24 h. The resulting films, with ABAME concentrations of 0.28, 0.57 and 1.4 mg/ml, were labeled as F1, F2 and F5, respectively. To remove the acid residues, both the dried blank film and chitosan-ABAME films were immersed in NaOH solution (1 M) for 20 min. After washing with approximately 350 ml of water to achieve neutrality (pH = 7), the films were dried at room temperature (22 ± 2 °C) for 24 h and stored in a desiccator.

2.3. Physicochemical characterization

2.3.1. Thermal analysis

Differential Scanning Calorimetry (DSC) curves were obtained on a DSC-60A (Shimadzu, Kyoto, Japan) using approximately 3 mg of sample in hermetically sealed aluminum crucibles under a dynamic nitrogen atmosphere (50 ml min^{-1}) and a heating rate of 10 °C.min^{-1} over a temperature range of 25–450 °C.

Thermogravimetry (TG) profiles were obtained using a DTG 60AH analyzer (Shimadzu) in a temperature range of 30–800 °C using alumina crucibles with approximately 5 mg of sample under a dynamic nitrogen atmosphere (50 ml min^{-1}) and a heating rate of 10 °C.min^{-1}.

2.3.2. Fourier transform infrared (FTIR) spectroscopy

The analysis was performed using an IRPrestige-21 spectrometer (Shimadzu) in the scanning wavenumber range from 4000 to 650 cm^{-1}. ABAME solid samples and films were placed directly in the equipment and analyzed by attenuated total reflectance (ATR).

2.3.3. X-ray diffraction (XRD)

XRD analyses were carried out on a D2 Phaser diffractometer (Bruker, MA, USA), with CuKα radiation (λ = 1.54 Å) at a voltage of 30 kV and a current of 10 mA, using a Lynxeye detector with 5°<2θ < 60° angular scanning. The samples were examined at room temperature for a period of 2 h at a scanning rate of 0.05°/s.

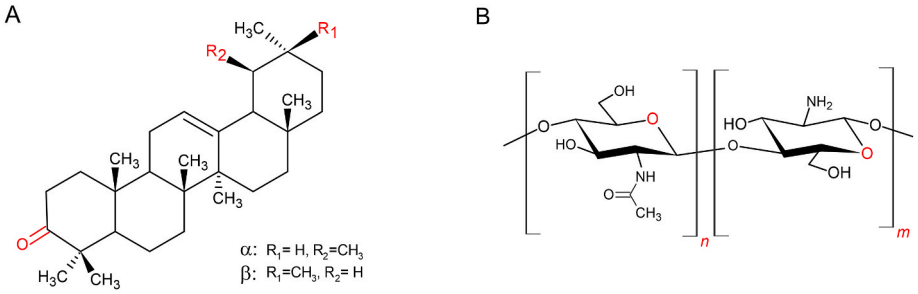

Fig. 1. Chemical structures of (A) α,β-amyrenone (ABAME) and (B) chitosan.

2.3.4. Scanning electron microscopy (SEM)

The morphological analysis of ABAME and films was carried out with a FEG Zeiss equipment, model Auriga (Carl Zeiss, Oberkochen, Germany), with magnification of 500X and 1500X. The samples were pretreated with the deposition of a gold layer on the surface, and the images were obtained with an acceleration potential of 5 kV under reduced pressure.

2.4. In vivo studies

2.4.1. Animals

In this research, fifty male Swiss mice (*Mus musculus*) aged 8–10 weeks, weighing between 25 and 35 g, were housed in the vivarium of the Health Sciences Center (CCS), in the annex of the Onofre Lopes University Hospital (HUOL/UFRN). Animals received food (pellets type feed) and water *ad libitum* throughout the tests, respecting the number of five animals per cage, and were kept at a temperature of 22 ± 2 °C, under a 12-h light-dark cycle. This study was approved by the Animal Experimentation Ethics Committee of the Federal University of Rio Grande do Norte, protocol number (210.080/2019).

Mice were randomly divided into five groups (n = 10 per group): untreated group (natural recovery, using only saline solution), BCF group (application of blank chitosan film) and CF1, CF2 and CF5 groups (treatment with chitosan-ABAME films F1, F2 and F5, respectively). Films applied were cut in a circular shape with a diameter of 1.0 cm and had ABAME concentrations of 0.11 mg/cm^2 (CF1), 0.23 mg/cm^2 (CF2) and 0.58 mg/cm^2 (CF5). Fig. 2 provides a schematic representation of *in vivo* experiments.

2.4.2. Wound induction

Animals were anesthetized intraperitoneally with 80 mg/kg ketamine and 10 mg/kg xylazine. After anesthesia, trichotomy (hair removal) was performed on the dorsal region to facilitate the visualization of the operative field as well as the analysis of the wound healing process. After asepsis, a circular excision, 1.0 cm in diameter, was done on the skin with the aid of a punch to expose the panniculus carnosus.

After injury induction, the film was applied immediately over the injured area, without any need to fix or reapply it, since it adhered to the injury site. After 7 and 14 days of treatment, mice were euthanized by intraperitoneal injection of 120 mg/kg ketamine and 30 mg/kg xylazine. At the end of this period, it was not necessary to remove the film because it was absorbed by the wound.

2.4.3. Macroscopic analysis

Wounds on the mice back were photographed in the postoperative period (0, 3, 7, 10 and 14 days), and their size was measured using the Image J software (National Institute of Health, Bethesda, MD, USA). The progression of healing, expressed as the percentage of wound closure, was calculated by the equation:

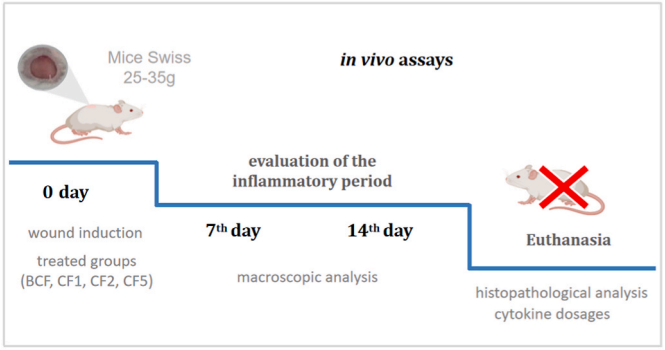

Fig. 2. Schematic representation of *in vivo* experiments.

$$\%\ Wound\ closure : \frac{Wa_0 - Wa_n}{Wa_0} \times 100 \quad (1)$$

where Wa_0 is the wound area (1 cm in diameter) at the start of the procedure (0 day) and Wa_n the wound area on the indicated day.

2.4.4. Histopathological analysis

After euthanasia of animals on the 7th and 14th days, wounds were excised with a margin of 2 mm beyond the edge of the wound for histopathological evaluation. For this, a representative sample was used to illustrate the wound healing observed in the present study.

For the histological analysis, samples of skin lesions in wounded animals were collected and immediately fixed in 10% formalin buffer (Dinâmica Química Contemporânea, São Paulo, SP, Brazil). After 24 h, samples were removed from formalin, dehydrated in six alcohol solutions at different concentrations (from 70 to 100%) for 1 h, and immersed in three xylene baths and subsequently in three paraffin baths. Samples were then submerged in paraffin to form blocks, from which 5 μm thick sections were cut in a microtome. Sections were finally fixed on slides, stained with hematoxylin and eosin, and later examined in an optical microscope, model BX50 (Olympus, Center Valley, PA, USA).

Based on the main results of the histopathological analysis of skin lesions on the 7th and 14th days of the experimental model, the following parameters were evaluated (Table 1): inflammatory infiltrate, re-epithelialization, neovascularization and areas of necrosis, which were classified using scores according to the protocol adapted by Abramov et al. [36].

2.4.5. Cytokine quantification analysis

The concentrations of cytokines interleukin 1β (IL1-β), interleukin 10 (IL-10) and Tumor Necrosis Factor α (TNF-α) were measured using a commercial enzyme immunoassay kit (R&D Systems, Minneapolis, MN, USA) and optical density measurements at 450 nm in a spectrophotometer (Mindray MR-96A, São Paulo, SP, Brazil). The wound tissue was homogenized in phosphate buffer-PBS (Dinâmica Química Contemporânea, São Paulo, SP, Brazil), pH 7.4, at a ratio of 1:5, and centrifuged at 4285 rpm for 10 min (Novatécnica NT 805, Piracicaba, SP, Brazil). The supernatant (100 μl) was then used to measure the markers [37]. The procedure was carried out in 96-well plates (Nunc-Immuno 96 MicroWell-Thermofisher, São Paulo, SP, Brazil), where samples were incubated for 18 h (overnight) at 4 °C together with the capture antibodies of IL-1β, IL-10 and TNF-α. The following day, plates were washed three times with PBS to remove the capture antibodies, and then samples were added to the plates and incubated for 2 h in a refrigerator at 4 °C together with detection antibodies. After adding the peroxidase conjugated solution, the plates were incubated for 20 min, and three more washes with PBS were made. A developing solution of tetramethylbenzidine with hydrogen peroxide and then a stop solution of H_2SO_4 (1 M) were finally added. All reagents were acquired from R&D Systems. The results were expressed in pg/ml [38].

2.4.6. Statistical analysis

The data obtained were expressed as means ± SD (standard deviation), and the differences among the groups were analyzed through one-way analysis of variance (ANOVA) followed by the Tukey post-test using the GraphPad Prism software, version 5.0 (GraphPad Software Inc., San

Table 1
Classification of criteria used in the histopathological analysis.

Score	Inflammatory infiltrate	Neovascularization	Re-epithelialization	Crust and necrosis
0	Absent	Absent	Absent	Absent
1	Discrete	Initial	Partial	Present
2	Moderate	Partial	Complete	–
3	Intense	Complete	–	–

Diego, CA, USA). Differences were considered statistically significant when $p \leq 0.05$.

3. Results and discussion

3.1. Physicochemical characterization

3.1.1. Differential scanning calorimetry

The DSC curve of ABAME revealed an endothermic event with T_{peak} at 104.97 °C (T_{onset} = 90.14 °C, T_{endset} = 115 °C) and an enthalpy value (ΔH) of −18.42 J/g, corresponding to its fusion (Fig. 3). A second endothermic event was observed with T_{peak} of 280.84 °C (T_{onset} = 195.09 °C, T_{endset} = 325.69 °C, ΔH = −2.52 kJ/g), which can be related ABAME decomposition [20]. On the other hand, the third endothermic peak with T_{peak} at 420.05 °C (T_{onset} = 410.85 °C, T_{endset} = 426.79 °C, ΔH = −8.28 J/g) can be ascribed, according to the literature, to the decomposition of carbonaceous compounds also found in other triterpenes [39].

The blank chitosan film (BCF) showed two events on its DSC curve, a first endothermic event with T_{peak} of 108.48 °C (T_{onset} = 87.79 °C, T_{endset} = 135.10 °C, ΔH = −191.23 J/g) due to water loss [40] and a second exothermic event related to chitosan decomposition, with T_{peak} at 271.69 °C (T_{onset} = 254.68 °C, T_{endset} = 286.17 °C, ΔH = 107.64 J/g).

The films, namely F1, F2 and F5, exhibited DSC patterns similar to those observed in BCF (Fig. 3C), i.e., endothermic events in the temperature range 70–140 °C ascribable to water loss, and exothermic events between 250 and 290 °C due to chitosan decomposition. Table 2 summarizes the main features of these events.

It is noteworthy that the F5 film also showed an endothermic event around 400 °C, which was probably due to decomposition of carbonaceous compounds present in the sample together with ABAME. It is likely that this event was evident only in F5 due to the highest concentration of ABAME used to prepare this film.

3.1.2. Thermogravimetric analysis

The thermogram of ABAME revealed a main event, starting at 210 °C and ending at 363 °C, with a loss of mass (Δm) of 98.9% (Fig. 3), which can be attributed to its decomposition. Another event can be observed more clearly in the Differential Thermal Analysis (DTA), with a small mass loss due to a secondary decomposition.

In the TG curve of BCF, a first mass loss event was found in the range 80–140 °C, corresponding to water loss. The second event at 240 °C, with Δm of 34.93%, corresponding to dehydration of sugar rings, decomposition and depolymerization of acetylated and deacetylated chitosan units [41], agrees with the exothermic event revealed by DTA and DSC.

The thermograms of films (Fig. 3D) showed an initial mass loss at approximately 100 °C due to water loss and a characteristic curve similar to that of BCF. Since the ABAME decomposition temperature was very close to that of chitosan, there was no significant change in this aspect. The percentage of mass loss in the range of 210–363 °C (23.69, 24.04 and 28.70% for F1, F2 and F5, respectively) was much lower than that of ABAME (Δm = 98.9%), thus demonstrating that films conferred greater thermal protection to the active principle.

Table 2
Description of the thermal events detected in DSC curves of F1, F2 and F5 films.

Film	Event	T_{onset} (°C)	T_{endset} (°C)	T_{peak} (°C)	ΔH (J/g)
F1	1st	67.26	106.76	89.21	−55.36
	2nd	254.11	285.51	271.82	45.84
F2	1st	72.26	108.65	94.15	−98.21
	2nd	255.46	286.42	272.28	33.21
F5	1st	49.62	107.48	85.99	−100.48
	2nd	252.84	286.89	267.19	45.49

3.1.3. Fourier transform infrared (FTIR) spectroscopy

The Fourier Transform Infrared (FTIR) spectrum of BCF showed a band between 3500 and 3050 cm^{-1}, corresponding to the –OH stretching, which overlapped, in the same region, with the –NH stretching (Fig. 4). While the bands found at 2920 and 2873 cm^{-1} can be ascribed to asymmetric and symmetric –CH stretching, that observed at 1645 cm^{-1} may have been due to C═O stretching of the acetylated amino group of chitin, thus suggesting its partial deacetylation to chitosan, and the ones at 1570 and 1375 cm^{-1} to N–H bending and C–N stretching, respectively. It was also possible to identify in the spectrum a peak at around 1316 cm^{-1} ascribable to the C–O bond of primary

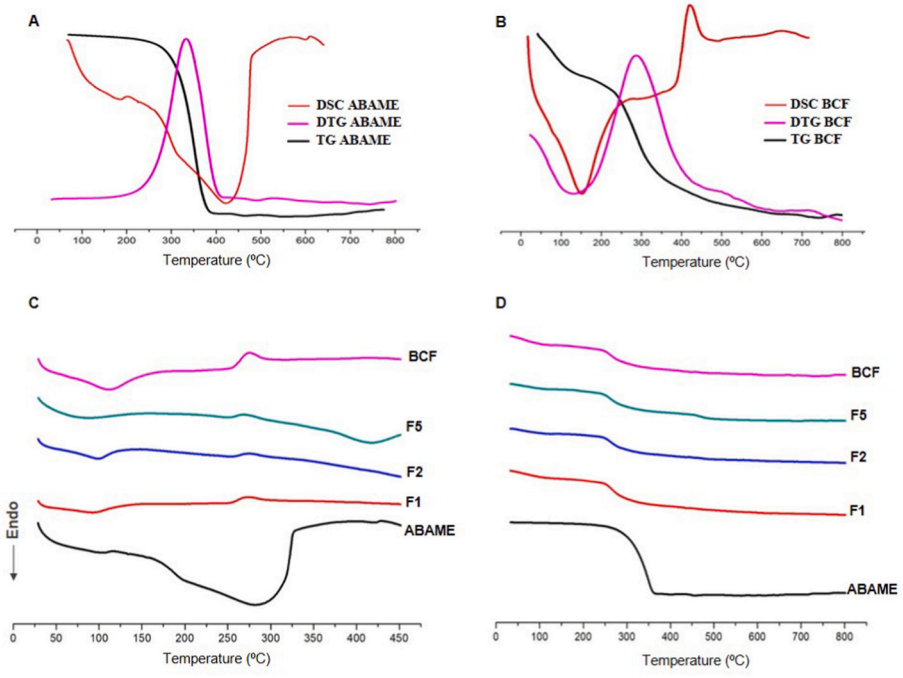

Fig. 3. Thermal DSC, TG and DTG analyses of (A) ABAME and (B) blank chitosan film (BCF); DSC (C) and TG (D) profiles of films.

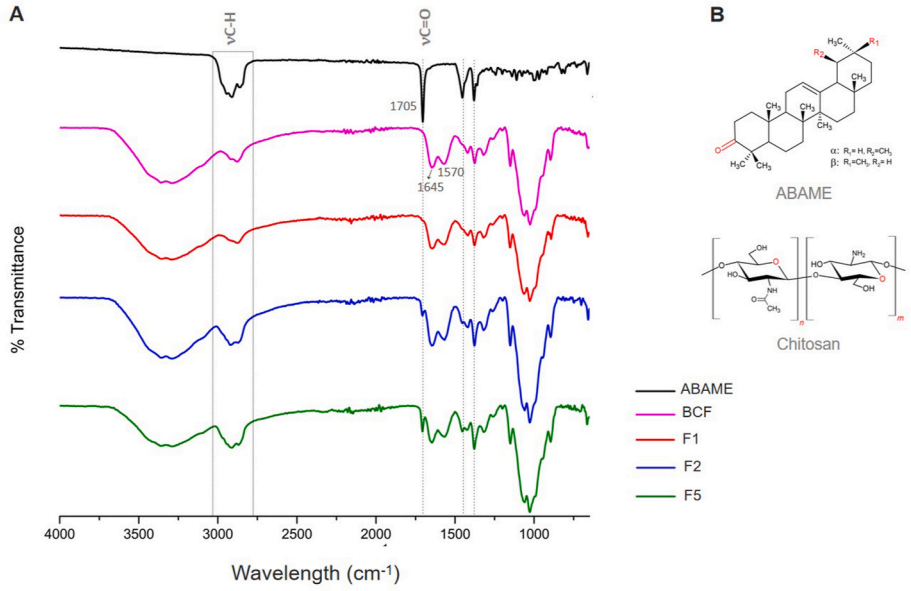

Fig. 4. (A) FTIR spectra of ABAME, blank chitosan film (BCF) and F1, F2 and F5 films. (B) Representations of ABAME and chitosan structures.

alcohols (–CH_2–OH) [39]. Other characteristic vibrational modes found in the region from 1153 to 900 cm^{-1} are typical of the stretching absorption of chitosan glycosidic ring.

Regarding the ABAME spectrum, the absorption band at 1705 cm^{-1} can be ascribed to C═O stretching, while bands in the region between 3050 and 2814 cm^{-1} are characteristic of C–H stretching of aromatic ring. Two other bands were found, at 1450 cm^{-1} and 1385 cm^{-1}, corresponding to –C-H deformation of methyl and methylene groups, respectively [20].

Chitosan-ABAME films had spectra similar to that of BCF, with the addition of some vibrational modes characteristic of ABAME, such as bands at 1450 and 1385 cm^{-1}, corresponding to –C-H deformation of methyl and methylene groups. Moreover, the C═O stretching at 1705 cm^{-1}, with the lowest intensity peak for F1 and the highest intensity one for F5, confirms the incorporation of ABAME at different concentrations in films.

3.1.4. X-ray diffraction (XRD)

The diffractogram of ABAME showed crystalline reflection in the region from 13° to 15°, thus suggesting its crystalline character (Fig. 5) and corroborating what was described by Ferreira et al. [20]. On the other hand, the absence of any crystalline reflection peaks in BCF diffractogram agrees with the amorphous state of chitosan films reported by Sun et al. [39].

The X-ray diffraction pattern of chitosan predominated in the diffractograms of F1, F2 and F5 likely due to ABAME inclusion in the chitosan matrix, which resulted in the loss of its crystalline profile and the predominance of the amorphous state.

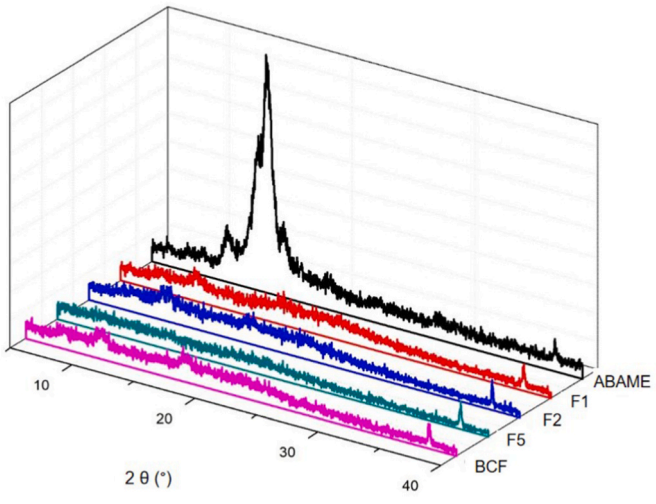

Fig. 5. X-ray diffraction patterns of ABAME, blank chitosan film (BCF), and F1, F2 and F5 films.

3.1.5. Scanning electron microscopy (SEM)

Scanning electron microscopy (SEM) images of ABAME confirmed the crystalline structure revealed by XRD (Fig. 6A and B). Contrariwise, the smooth, uniform and compact surface of BCF (Fig. 6I) is in agreement with other studies that reported no crystalline structure for chitosan films [42].

One can identify, in the micrographs of F1, F2 and F5, ABAME particles homogeneously dispersed in the chitosan matrix, but without the characteristic crystalline structure of ABAME. These results not only agree with the loss of ABAME crystallinity in films revealed by XRD, but also confirm the inclusion of the active principle in the polymer matrix.

3.2. In vivo study

3.2.1. Wound healing activity

The macroscopic analysis illustrated in Fig. 7A shows the wound healing progression in lesions on the back of mice. It can be seen that animals treated with chitosan-ABAME films (CF1, CF2 and CF5 groups) benefited from a much more effective and faster regeneration process than the untreated group and BCF.

The skin lesions (Fig. 7B) observed 7 and 10 days after injury had significantly different areas, with mean values of wound closure percentage of approximately 17 and 48% in the untreated group, and 19 and 54% in the BCF one, respectively. In contrast, the CF1 group exhibited values of around 62 and 87%, the CF2 group of 54 and 84%, and the CF5 one of 54 and 86% after 7 and 10 days, respectively. Therefore, groups treated with chitosan-ABAME films showed a superior wound-healing effect than untreated and BCF-treated groups.

As is well known, cyclo-oxygenase 2 (COX-2) produced in inflammatory processes is an enzyme that converts arachidonic acid into prostaglandins, prostacyclins and thromboxanes, whose action can be

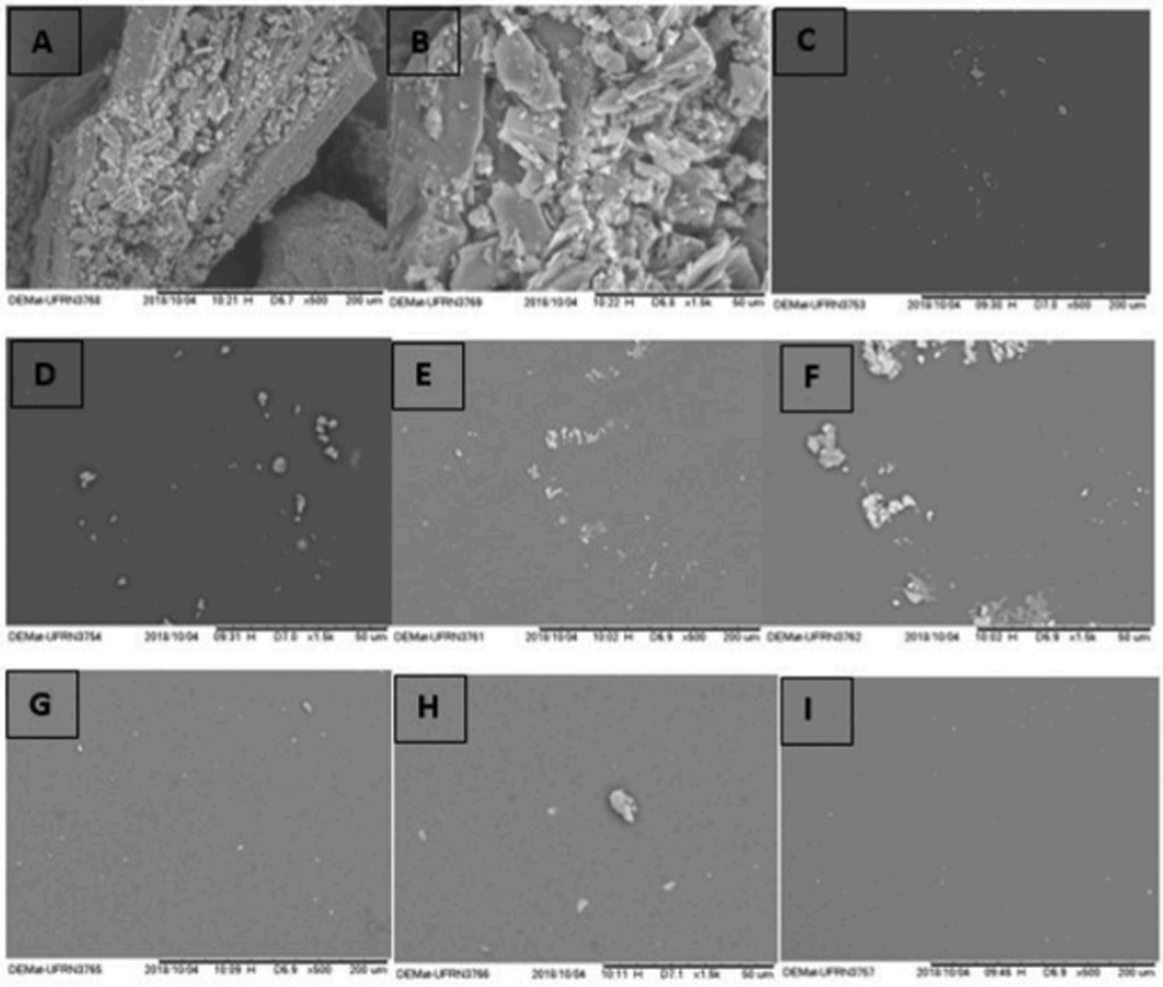

Fig. 6. SEM images of (A) ABAME 500X, (B) ABAME 1500X, (C) F1 500X, (D) F1 1500X, (E) F2 500X, (F) F2 1500X, (G) F5 500X, (H) F5 1500X and (I) blank chitosan film 500X.

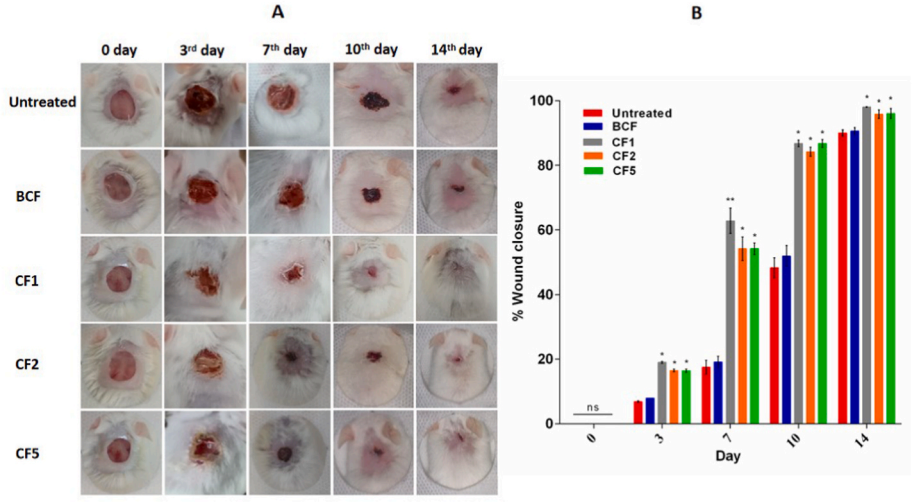

Fig. 7. *In vivo* wound healing study performed on the dorsum of Swiss mice on the 3rd, 7th and 14th days. Results refer to the untreated group and groups BCF, CF1, CF2 and CF5. (A) Macroscopic images of skin wound. (B) Wound closure expressed as the percentage of wound closure in relation to the original size along the postoperative time.

inhibited by anti-inflammatory drugs such as non-steroidal anti-inflammatory drugs (NSAIDs) [43]. In this sense, the triterpenes class has several pharmacological activities, including a topical anti-inflammatory effect. It is also known that the mixture of α- and β-amyrins (precursors of ABAME) is capable of reducing the level of prostaglandin E2 by suppressing COX-2 expression, thereby inhibiting the signs of the inflammatory process [44]. Therefore, based on the above results and according to what was reported in the literature [20,45], it can be inferred that such an ABAME anti-inflammatory activity may have contributed to the observed wound healing.

3.2.2. Histopathological analysis

In the histopathological analysis carried out on the 7th day after injury, the untreated and BCF-treated groups showed an area of edema, intense inflammatory infiltrate and granulation, in addition to the formation of crust and punctual areas of necrosis (Fig. 8). However, the BCF group also showed a more organized tissue when compared to the untreated one. In the groups treated with chitosan-ABAME films (CF1, CF2 and CF5), there was a moderate inflammatory infiltrate and an abundant angiogenesis (new vessels).

In turn, making reference to the 14th day (Fig. 8), the untreated and BCF-treated groups showed partial re-epithelialization and moderate inflammatory infiltrate, while the CF1, CF2 and CF5 ones complete re-epithelialization, dermal remodeling and neovascularization. Moreover, in some samples there was an inflammatory infiltrate, even if discrete and punctual.

According to the results illustrated in Fig. 9, the CF1, CF2 and CF5 groups showed higher levels of re-epithelialization and neovascularization compared to the other groups on the 7th and 14th days. In addition, the levels of inflammatory infiltrate in groups that received chitosan-ABAME films were lower than those in the BCF-treated and untreated ones. BCF was shown to be effective in improving re-epithelialization and neovascularization as well.

Finally, the groups treated with chitosan-ABAME films showed qualitative and quantitative improvement in wound healing, when compared to the group treated only with BCF and the untreated one.

3.2.3. Cytokine quantification

Cytokines are part of a group of proteins that mediate responses to innate and acquired immunity. Synthesized at the injured site in response to an inflammatory or antigenic stimulus, they can be classified into pro-inflammatory and anti-inflammatory cytokines [46]. Anti-inflammatory cytokines act inhibiting the immune response, helping in the wound healing process, while the pro-inflammatory ones are overproduced in response to an injury or infection [38].

TNF-α is a pro-inflammatory cytokine that, at high concentrations, acts in the inflammatory cascade, generating other inflammation and tissue destruction mediators [47]. In turn, IL-1β is responsible for triggering a systemic inflammatory process that activates COX-2, inducing the formation of prostaglandin E2 as well as the productions of nitric oxide and endothelial adhesion molecules [48]. IL-10 is an anti-inflammatory cytokine responsible for inhibiting the pro-inflammatory cytokines and stimulating the endogenous production of other anti-inflammatory cytokines.

The levels of TNF-α, IL-1β and IL-10 cytokines detected after 7 and 14 days of treatment of mice lesion are depicted in Fig. 10. The untreated group showed high levels of TNF-α, both on the 7th and 14th days of therapy, while a reduction in its level was observed mainly on the 14th day in the BCF group. However, the greatest reductions in TNF-α levels occurred in CF1, CF2 and CF5 groups ($p < 0.01$).

Although the IL-1β levels were similar to those of TNF-α, their largest reductions occurred mainly on the 7th day of therapy in groups submitted to treatment (BCF, F1, F2 and F5) when compared to the untreated group.

IL-10 levels in the untreated group were much lower than in the other groups, both on the 7th and 14th days. Particularly, an increase in these levels was observed mainly in groups submitted to treatment with chitosan-ABAME films, but even in the BCF group, especially on the 7th day of therapy.

It can be observed that TNF-α was induced as a result of an inflammatory stimulus (skin lesion), and, in turn, IL-10, which was produced in higher concentration by groups submitted to treatment with chitosan-ABAME films, caused a greater reduction in TNF-α production. This observation indicates the establishment of the homeostasis mechanism involved between IL-10 cytokines and pro-inflammatory cytokines, according to the resolution of the inflammatory process [46,49].

In short, the results obtained in *in vivo* studies indicated that, although films F2 (0.57 mg/ml) and F5 (1.4 mg/ml) had different concentrations of the active compound, they showed very similar results. However, sometimes the less concentrated film performed even better than the more concentrated one. The use of two different concentrations of the active compound had the aim of identifying the one capable of ensuring the maximum response; therefore, the results obtained indicate a starting point to establish the optimal dose of active compound in future formulations.

In the chitosan-ABAME combination we sought a synergism of the properties of the two components, among which antimicrobial activity, low toxicity, biodegradation, chitosan biocompatibility and ABAME anti-inflammatory activity, aiming to maximize the pharmacological potential of the resulting drug-loaded film. Finally, the final composite,

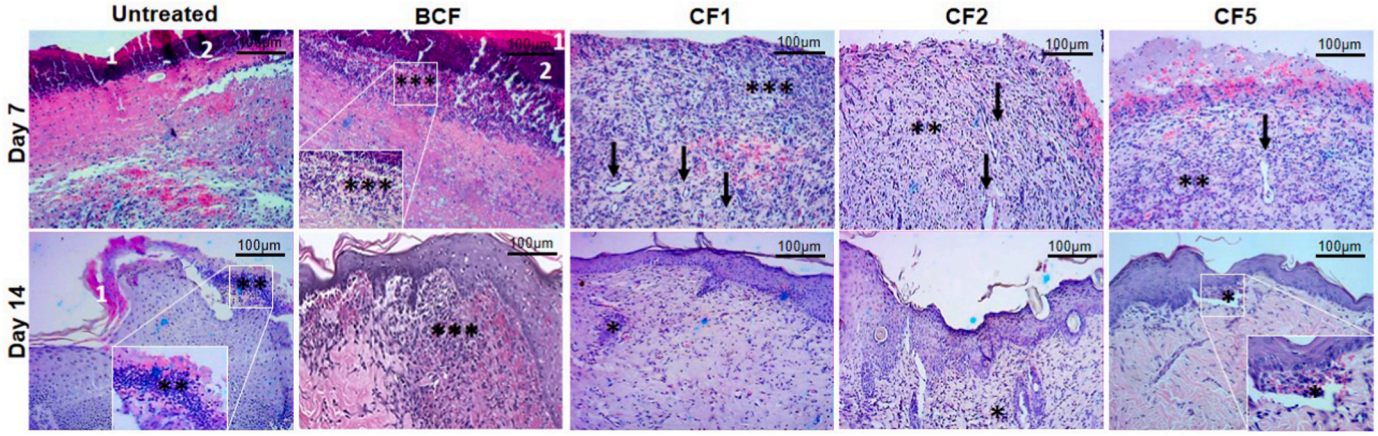

Fig. 8. Representative images of the histopathological analysis of mice lesions on the 7th and 14th experimental days. Results referring to the untreated group and treated groups (BCF, CF1, CF2 and CF5): (1) crust, (2) points with necrosis, (↓) neovascularization, (*) discrete inflammatory infiltrate, (**) moderate inflammatory infiltrate, (***) intense inflammatory infiltrate.

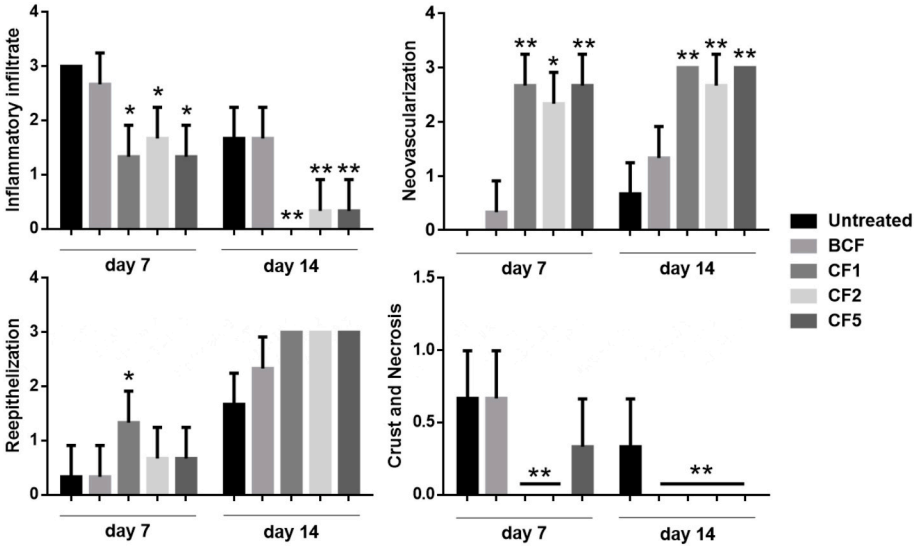

Fig. 9. Histomorphology of stained epithelial tissue from the untreated group and treated groups (BCF, CF1, CF2 and CF5), after 7 and 14 days. The following characteristics were evaluated: inflammatory infiltrate, neovascularization, re-epithelialization, crust and necrosis. Statistical difference was checked by ANOVA followed by the Tukey post-test. Data are the average of values obtained in five animals. **$p < 0.001$ and * $p < 0.01$ for comparison among groups.

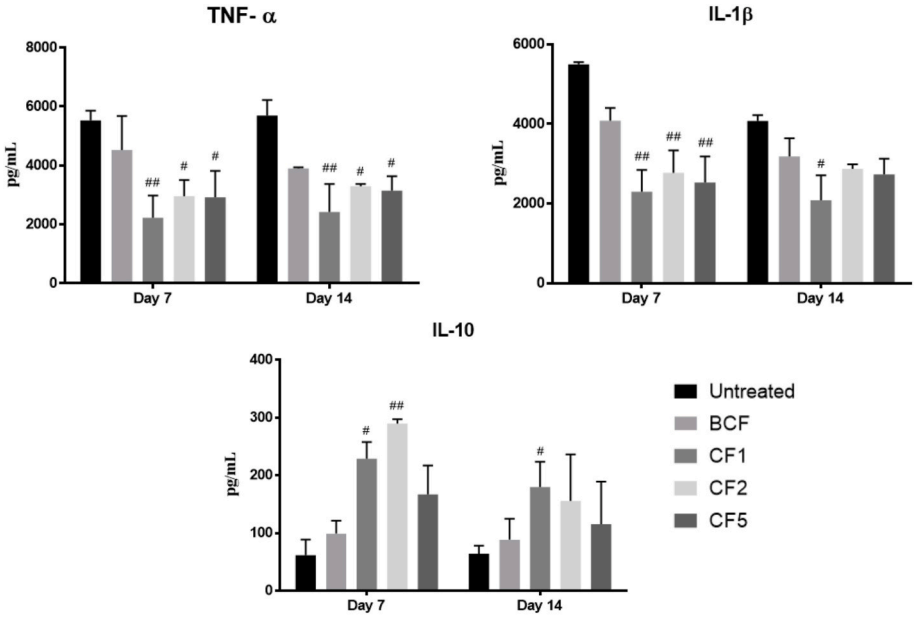

Fig. 10. Levels of tumor necrosis factor (TNF–α) and of interleukins IL-1β and IL-10 on days 7 and 14 of therapy. The results are presented as mean value ± standard error of the mean (n = 5). $^{\#}p < 0.01$ $^{\#\#}p < 0.001$ vs. the untreated group (ANOVA followed by the Tukey post-test).

to be used as a skin formulation, would have, as peculiarity, the incorporation of a natural Amazonian active principle with great biological potential.

4. Conclusions

The selected sol-gel solvent evaporation method allowed the efficient development of chitosan-α,β-amyrenone (ABAME) films with good physical appearance and smooth and homogeneous surface. The physicochemical results demonstrated ABAME inclusion in the chitosan matrix in three different concentrations. Particularly, the FTIR spectra showed the characteristic bands of the active compound in the films, the X-ray diffractograms remarkable changes in the ABAME crystalline profile, and the scanning electron micrographs a well distribution of ABAME particles in the polymer chitosan matrix as well as changes in the crystalline appearance.

The *in vivo* tests carried out using chitosan-ABAME films showed complete closure of wounds in the back of mice on the 14th day of treatment, leading to re-epithelialization, stimulation of angiogenesis (neovascularization) and expression of cytokines that contributed to the healing and deinflammation process. These results were significantly better than those observed in the untreated group and the group treated with chitosan blank film. It was not expected that the increase in the active compound dose would necessarily result in a proportional activity improvement. Since F2 and F5 films showed similar results, they provide us with a good dose perspective for the development of future formulations.

As a whole, the results of this study demonstrated that ABAME-loaded chitosan films allowed to regenerate lesions induced in mice, showing a great wound healing potential.

CRediT authorship contribution statement

Ulana Cristina de Araújo Tavares: Investigation, Methodology, Writing – original draft. **Juliana Maria Nascimento dos Santos:** Methodology, Writing – original draft. **Sávio Gorgônio Paes de Bulhões:** Methodology. **Lucas Gabriel de Medeiros da Silva:** Methodology. **Verônica da Silva Oliveira:** Writing – review & editing. **Emanuella de Aragão Tavares:** Methodology, Formal analysis. **Raimundo Fernandes de Araújo Júnior:** Formal analysis. **Valéria Costa da Silva:** Formal analysis. **Gerlane Coelho Bernardo Guerra:** Formal analysis. **Emerson Silva Lima:** Methodology. **Valdir Florêncio da Veiga Júnior:** Methodology. **Attilio Converti:** Writing – review & editing. **Ádley Antonini Neves de Lima:** Conceptualization, Writing – review & editing, Supervision, Project administration, Funding acquisition.

Declaration of competing interest

The authors declare no competing interest.

Data availability

All data generated or analyzed during this study are included in this study, and the original data are available upon request.

Acknowledgements

The authors thank the Coordination for the Improvement of Higher Education Personnel (CAPES) and the National Council for Scientific and Technological Development (CNPq) for their financial support.

References

[1] B. Bednarczyk-Cwynar, N. Wachowiak, M. Szulc, E. Kaminska, A. Bogacz, J. Bartkowiak-Wieczorek, L. Zaprutko, P.L. Mikolajczak, Strong and long-lasting antinociceptive and anti-inflammatory conjugate of naturally occurring oleanolic acid and aspirin, Front. Pharmacol. 7 (2016) 202, https://doi.org/10.3389/fphar.2016.00202.

[2] G. Renda, İ. Gökkaya, D. Şöhretoğlu, Immunomodulatory properties of triterpenes, Phytochemistry Rev. 21 (2022) 537–563, https://doi.org/10.1007/s11101-021-09785-x.

[3] N.N.E. El-Sayed, A.M. Alafeefy, M.A. Bakht, V.H. Masand, A. Aldalbahi, N. Chen, C. Fan, A. Ben Bacha, Synthesis, antiphospholipase A2, antiprotease, antibacterial evaluation and molecular docking analysis of certain novel hydrazones, Molecules 21 (2016) 1664, https://doi.org/10.3390/molecules21121664.

[4] S. Rahimi, J. Kim, I. Mijakovic, K.H. Jung, G. Choi, S.C. Kim, Y.J. Kim, Triterpenoid-biosynthetic UDP-glycosyltransferases from plants, Biotechnol. Adv. 37 (2019), 107394, https://doi.org/10.1016/j.biotechadv.2019.04.016.

[5] J.A.R. Salvador, A.S. Leal, A.S. Valdeira, B.M.F. Gonçalves, D.P.S. Alho, S.A. C. Figueiredo, S.M. Silvestre, V.I.S. Mendes, Oleanane-, ursane-, and quinone methide friedelane-type triterpenoid derivatives: recent advances in cancer treatment, Eur. J. Med. Chem. 142 (2017) 95–130, https://doi.org/10.1016/j.ejmech.2017.07.013.

[6] Ł. Woźniak, S. Skąpska, K. Marszałek, Ursolic acid - a pentacyclic triterpenoid with a wide spectrum of pharmacological activities, Molecules 20 (2015) 20614–20641, https://doi.org/10.3390/molecules201119721.

[7] D. Kemboi, X. Peter, M. Langat, J. Tembu, A review of the ethnomedicinal uses, biological activities, and triterpenoids of Euphorbia species, Molecules 25 (2020) 4019, https://doi.org/10.3390/molecules25174019.

[8] G.B. Xu, Y.H. Xiao, Q.Y. Zhang, M. Zhou, S.G. Liao, Hepatoprotective natural triterpenoids, Eur. J. Med. Chem. 145 (2018) 691–716, https://doi.org/10.1016/j.ejmech.2018.01.011.

[9] J.M. Castellano, S. Ramos-Romero, J.S. Perona, Oleanolic acid: extraction, characterization and biological activity, Nutrients 14 (2022) 1–29, https://doi.org/10.3390/nu14030623.

[10] M.B. Isah, M.A. Ibrahim, A. Mohammed, A.B. Aliyu, B. Masola, T.H.T. Coetzer, A systematic review of pentacyclic triterpenes and their derivatives as chemotherapeutic agents against tropical parasitic diseases, Parasitology 143 (2016) 1219–1231, https://doi.org/10.1017/S0031182016000718.

[11] C.H.L. Dinh, A. Szabo, D. Camer, Y. Yu, H. Wang, X.F. Huang, Bardoxolone methyl prevents fat deposition and inflammation in the visceral fat of mice fed a high-fat diet, Chem. Biol. Interact. 229 (2015) 1–8, https://doi.org/10.1016/j.cbi.2015.01.025.

[12] N.N.M. Razali, C.T. Ng, L.Y. Fong, Cardiovascular protective effects of Centella asiatica and its triterpenes: a review, Planta Med. 85 (2019) 1203–1215, https://doi.org/10.1055/a-1008-6138.

[13] G.A. Gutiérrez-Rebolledo, A.G. Siordia-Reyes, M. Meckes-Fischer, A. Jiménez-Arellanes, Hepatoprotective properties of oleanolic and ursolic acids in antitubercular drug-induced liver damage, Asian Pac. J. Tropical Med. 9 (2016) 644–651, https://doi.org/10.1016/j.apjtm.2016.05.015.

[14] Y.J. Ding, C.Y. Sun, C.C. Wen, Y.H. Chen, Nephroprotective role of resveratrol and ursolic acid in aristolochic acid intoxicated zebrafish, Toxins 7 (2015) 97–109, https://doi.org/10.3390/toxins7010097.

[15] X.-B. Huang, Y.-J. Chen, W.-Q. Chen, N.-Q. Wang, X.-L. Wu, Y. Liu, Neuroprotective effects of tenuigenin on neurobehavior, oxidative stress, and tau hyperphosphorylation induced by intracerebroventricular streptozotocin in rats, Brain Circ 4 (2018) 24, https://doi.org/10.4103/bc.bc_2_17.

[16] P. Wu, J. Zheng, T. Huang, D. Li, Q. Hu, A. Cheng, Z. Jiang, L. Jiao, S. Zhao, K. Zhang, Synthesis and evaluation of novel triterpene analogues of ursolic acid as potential antidiabetic agent, PLoS One 10 (2015) 1–15, https://doi.org/10.1371/journal.pone.0138767.

[17] H. Lou, H. Li, S. Zhang, H. Lu, Q. Chen, A review on preparation of betulinic acid and its biological activities, Molecules 26 (2021) 5583, https://doi.org/10.3390/molecules26185583.

[18] R. Gomes, F. Guilhon-simplicio, L.D. Rosales, N.Y. Batista, F.C. Guedes-junior, M. Silva, L. Ferreira, Anti-hyperglycemic, Lipid-Lowering, and Anti-obesity Effects of the Triterpenes α and β-amyrenones in Vivo, vol. 11, 2021, pp. 451–463, https://doi.org/10.22038/AJP.2021.18076.

[19] J. Hodon, L. Borkova, J. Pokorny, A. Kazakova, M. Urban, Design and synthesis of pentacyclic triterpene conjugates and their use in medicinal research, Eur. J. Med. Chem. 182 (2019), 111653, https://doi.org/10.1016/j.ejmech.2019.111653.

[20] R.G.S. Ferreira, W.F. Silva, V.F. Veiga, Á.A.N. Lima, E.S. Lima, Physicochemical characterization and biological activities of the triterpenic mixture α,β-amyrenone, Molecules 22 (2017) 298, https://doi.org/10.3390/molecules22020298.

[21] E.M. Lima, A.M. Nascimento, D. Lenz, R. Scherer, S.S. Meyrelles, G.A.P. Boëchat, T. U. Andrade, D.C. Endringer, Triterpenes from the protium heptaphyllum resin – chemical composition and cytotoxicity, Rev. Bras. Farmacogn. 24 (2014) 399–407, https://doi.org/10.1016/j.bjp.2014.06.003.

[22] P.F. Rosalem, T.B. Picão, F.C. Rodrigues-Lisoni, A.R. Martins, Leaf anatomy of Protium ovatum and its antiproliferative potential in cervical cells, Rev. Bras. Farmacogn. 27 (2017) 673–678, https://doi.org/10.1016/j.bjp.2017.09.001.

[23] N.L.M. Quintão, L.W. Rocha, G.F. Silva, S. Reichert, V.D. Claudino, R.M. Lucinda-Silva, A. Malheiros, M.M. De Souza, V.C. Filho, T.M. Bellé Bresolin, M.D. S. Machado, T.M. Wagner, C. Meyre-Silva, Contribution of α, β -amyrenone to the anti-inflammatory and antihypersensitivity effects of Aleurites moluccana (L.) Willd, BioMed Res. Int. 2014 (2014), https://doi.org/10.1155/2014/636839.

[24] P.D.O. De Almeida, A.P.D.A. Boleti, A.L. Rüdiger, G.A. Lourenço, V. Florêncio, E. S. Lima, Anti-inflammatory activity of triterpenes isolated from protium paniculatum oil-resins, 2015 (2015), Evid. Based Complement. Alternat. Med. 2015 (2015), 293768, https://doi.org/10.1155/2015/293768.2015.

[25] S. Sut, F. Maggi, M. Nicoletti, V. Baldan, S. Dall'Acqua, New drugs from old natural compounds: scarcely investigated sesquiterpenes as new possible therapeutic agents, Curr. Med. Chem. 25 (2018) 1241–1258, https://doi.org/10.2174/0929867324666170404150351.

[26] Z. Özdemir, Z. Wimmer, Selected plant triterpenoids and their amide derivatives in cancer treatment: a review, Phytochemistry 203 (2022), 113340, https://doi.org/10.1016/J.PHYTOCHEM.2022.113340.

[27] S.A. Bhat, S.N. Kazim, A road to contemporary era of hepatitis B virus regimen replacing existing therapeutics exploiting plant secondary metabolites as emerging heroes in exploring drugs: an expedition for a functional cure, Gene Reports 30 (2023), 101743, https://doi.org/10.1016/J.GENREP.2023.101743.

[28] C. Kamaraj, C. Ragavendran, R.C.S. Kumar, A. Ali, S.U. Khan, Z. ur R. Mashwani, J. P. Luna-Arias, J.P.R. Pedroza, Antiparasitic potential of asteraceae plants: a comprehensive review on therapeutic and mechanistic aspects for biocompatible drug discovery, Phytomedicine 2 (2022), 100377, https://doi.org/10.1016/J.PHYPLU.2022.100377.

[29] W. Wang, Q. Meng, Q. Li, J. Liu, M. Zhou, Z. Jin, K. Zhao, Chitosan derivatives and their application in biomedicine, Int. J. Mol. Sci. 21 (2020) 487, https://doi.org/10.3390/ijms21020487.

[30] L. Bedian, A.M. Villalba-Rodríguez, G. Hernández-Vargas, R. Parra-Saldivar, H.M. N. Iqbal, Bio-based materials with novel characteristics for tissue engineering applications – a review, Int. J. Biol. Macromol. 98 (2017) 837–846, https://doi.org/10.1016/j.ijbiomac.2017.02.048.

[31] J. Lizardi-Mendoza, W.M. Argüelles Monal, F.M. Goycoolea Valencia, Chemical characteristics and functional properties of chitosan, in: Chitosan Preserv. Agric. Commod., Elsevier, 2016, pp. 3–31, https://doi.org/10.1016/B978-0-12-802735-6.00001-X.

[32] S. Alven, B.A. Aderibigbe, Chitosan and cellulose-based hydrogels for wound management, Int. J. Mol. Sci. 21 (2020) 1–30, https://doi.org/10.3390/ijms21249656.

[33] H.L. Loo, B.H. Goh, L.H. Lee, L.H. Chuah, Application of chitosan-based nanoparticles in skin wound healing, Asian J. Pharm. Sci. 17 (2022) 299–332, https://doi.org/10.1016/j.ajps.2022.04.001.

[34] K. Azuma, R. Izumi, T. Osaki, S. Ifuku, M. Morimoto, H. Saimoto, S. Minami, Y. Okamoto, Chitin, chitosan, and its derivatives for wound healing: old and new materials, J. Funct. Biomater. 6 (2015) 104–142, https://doi.org/10.3390/jfb6010104.

[35] I. Aranaz, R. Harris, F. Navarro-García, A. Heras, N. Acosta, Chitosan based films as supports for dual antimicrobial release, Carbohydr. Polym. 146 (2016) 402–410, https://doi.org/10.1016/j.carbpol.2016.03.064.

[36] Y. Abramov, B. Golden, M. Sullivan, S.M. Botros, J.J.R. Miller, A. Alshahrour, R. P. Goldberg, P.K. Sand, Histologic characterization of vaginal vs. abdominal

surgical wound healing in a rabbit model, Wound Repair Regen. 15 (2007) 80–86, https://doi.org/10.1111/j.1524-475X.2006.00188.x.
[37] B. Safieh-Garabedian, S. Poole, A. Allchorne, J. Winter, C.J. Woolf, Contribution of interleukin-1β to the inflammation-induced increase in nerve growth factor levels and inflammatory hyperalgesia, Br. J. Pharmacol. 115 (1995) 1265–1275, https://doi.org/10.1111/j.1476-5381.1995.tb15035.x.
[38] A.A. Araújo, T.O. Souza, L.M. Moura, G.A.C. Brito, K.S. Aragão, L.S. Araújo, C.A. X. Medeiros, M.S.C.F. Alves, R.F. Araújo, Effect of telmisartan on levels of IL-1, TNF-α, down-regulated COX-2, MMP-2, MMP-9 and RANKL/RANK in an experimental periodontitis model, J. Clin. Periodontol. 40 (2013) 1104–1111, https://doi.org/10.1111/jcpe.12160.
[39] L. Sun, J. Sun, L. Chen, P. Niu, X. Yang, Y. Guo, Preparation and characterization of chitosan film incorporated with thinned young apple polyphenols as an active packaging material, Carbohydr. Polym. 163 (2017) 81–91, https://doi.org/10.1016/j.carbpol.2017.01.016.
[40] S. Shankar, L.F. Wang, J.W. Rhim, Preparation and properties of carbohydrate-based composite films incorporated with CuO nanoparticles, Carbohydr. Polym. 169 (2017) 264–271, https://doi.org/10.1016/j.carbpol.2017.04.025.
[41] S. Mathew, M. Brahmakumar, T.E. Abraham, Microstructural imaging and characterization of the mechanical, chemical, thermal, and swelling properties of starch-chitosan blend films, Biopolymers 82 (2006) 176–187, https://doi.org/10.1002/bip.20480.
[42] S. Hajji, A. Chaker, M. Jridi, H. Maalej, K. Jellouli, S. Boufi, M. Nasri, Structural analysis, and antioxidant and antibacterial properties of chitosan-poly (vinyl alcohol) biodegradable films, Environ. Sci. Pollut. Res. 23 (2016) 15310–15320, https://doi.org/10.1007/s11356-016-6699-9.
[43] P.H. Wang, B.S. Huang, H.C. Horng, C.C. Yeh, Y.J. Chen, Wound healing, J. Chin. Med. Assoc. 81 (2018) 94–101, https://doi.org/10.1016/j.jcma.2017.11.002.
[44] Y. Wang, J. Li, Y. Huang, X. Dai, Y. Liu, Z. Liu, Y. Wang, N. Wang, P. Zhang, Tripartite motif-containing 28 bridges endothelial inflammation and angiogenic activity by retaining expression of TNFR-1 and -2 and VEGFR2 in endothelial cells, Faseb. J. 31 (2017) 2026–2036, https://doi.org/10.1096/fj.201600988RR.
[45] X. Niu, H. Yao, W. Li, Q. Mu, H. Li, H. Hu, Y. Li, H. Huang, δ-Amyrone, a specific inhibitor of cyclooxygenase-2, exhibits anti-inflammatory effects in vitro and in vivo of mice, Int. Immunopharm. 21 (2014) 112–118, https://doi.org/10.1016/j.intimp.2014.04.019.
[46] C. Qing, The molecular biology in wound healing & non-healing wound, Chinese J. Traumatol. - English Ed. 20 (2017) 189–193, https://doi.org/10.1016/j.cjtee.2017.06.001.
[47] S.Y. Kim, M.G. Nair, Macrophages in wound healing: activation and plasticity, Immunol. Cell Biol. 97 (2019) 258–267, https://doi.org/10.1111/imcb.12236.
[48] H. Kansu-Celik, O. Gun-Eryılmaz, N.U. Dogan, S. Haktankaçmaz, M. Cinar, S. S. Yilmaz, C. Gülerman, Prostaglandin E2 induction of labor and cervical ripening for term isolated oligohydramnios in pregnant women with Bishop score $\leq$ 5, J. Chin. Med. Assoc. 80 (2017) 169–172, https://doi.org/10.1016/j.jcma.2016.07.004.
[49] N. Navaei-Alipour, M. Mastali, G.A. Ferns, M. Saberi-Karimian, M. Ghayour-Mobarhan, The effects of honey on pro- and anti-inflammatory cytokines: a narrative review, Phyther. Res. 35 (2021) 3690–3701, https://doi.org/10.1002/ptr.7066.